

Interaction between Amyloid Beta Peptide and an Aggregation Blocker Peptide Mimicking Islet Amyloid Polypeptide

Nasrollah Rezaei-Ghaleh¹, Erika Andreetto², Li-Mei Yan², Aphrodite Kapurniotu², Markus Zweckstetter^{1,3*}

1 Department for NMR-based Structural Biology, Max-Planck-Institute for Biophysical Chemistry, Göttingen, Germany, **2** Division of Peptide Biochemistry, Technische Universität München, Freising, Germany, **3** DFG Research Center for the Molecular Physiology of the Brain (CMPB), Göttingen, Germany

Abstract

Assembly of amyloid-beta peptide (A β) into cytotoxic oligomeric and fibrillar aggregates is believed to be a major pathologic event in Alzheimer's disease (AD) and interfering with A β aggregation is an important strategy in the development of novel therapeutic approaches. Prior studies have shown that the double N-methylated analogue of islet amyloid polypeptide (IAPP) IAPP-GI, which is a conformationally constrained IAPP analogue mimicking a non-amyloidogenic IAPP conformation, is capable of blocking cytotoxic self-assembly of A β . Here we investigate the interaction of IAPP-GI with A β 40 and A β 42 using NMR spectroscopy. The most pronounced NMR chemical shift changes were observed for residues 13–20, while residues 7–9, 15–16 as well as the C-terminal half of A β - that is both regions of the A β sequence that are converted into β -strands in amyloid fibrils - were less accessible to solvent in the presence of IAPP-GI. At the same time, interaction of IAPP-GI with A β resulted in a concentration-dependent co-aggregation of A β and IAPP-GI that was enhanced for the more aggregation prone A β 42 peptide. On the basis of the reduced toxicity of the A β peptide in the presence of IAPP-GI, our data are consistent with the suggestion that IAPP-GI redirects A β into nontoxic "off-pathway" aggregates.

Citation: Rezaei-Ghaleh N, Andreetto E, Yan L-M, Kapurniotu A, Zweckstetter M (2011) Interaction between Amyloid Beta Peptide and an Aggregation Blocker Peptide Mimicking Islet Amyloid Polypeptide. PLoS ONE 6(5): e20289. doi:10.1371/journal.pone.0020289

Editor: Janine Santos, University of Medicine and Dentistry of New Jersey, United States of America

Received: November 29, 2010; **Accepted:** April 29, 2011; **Published:** May 25, 2011

Copyright: © 2011 Rezaei-Ghaleh et al. This is an open-access article distributed under the terms of the Creative Commons Attribution License, which permits unrestricted use, distribution, and reproduction in any medium, provided the original author and source are credited.

Funding: This work was supported by the Max Planck Society and the DFG through a Heisenberg scholarship (ZW 71/2-2 and 3-2) to M.Z. The funders had no role in study design, data collection and analysis, decision to publish, or preparation of the manuscript.

Competing Interests: The authors have declared that no competing interests exist.

* E-mail: mzwecks@gwdg.de

Introduction

Protein misfolding and aggregation into amyloid fibrillar aggregates are associated with a number of severe neurodegenerative diseases including Alzheimer's disease (AD) [1]. The main pathological hallmarks of AD are the extracellular "senile plaques", constituted of amyloid β (A β) peptide, and the intracellular "neurofibrillary tangles" of tau protein [2]. Several genetic and pathologic evidences support the "amyloid cascade hypothesis" of AD, according to which A β peptide self-association plays a vital initiating role in AD pathogenesis, both in familial and sporadic forms of disease [3,4]. A β peptide constitutes a small part of a large transmembrane protein, the amyloid precursor protein (APP), and is released to the extracellular environment after two consecutive proteolytic cleavages of APP by β - and γ -secretase [5]. The 39–42 residue A β peptide is mostly unstructured in aqueous solution [6–8], but has a tendency to undergo a conformational transition to β -sheet aggregates [9]. This self-association of A β is known to exert its neurotoxic effects [10]. While the final amyloid fibrillar state of A β was originally believed to cause the main toxic effects of this peptide, increasing evidence suggests that the earliest and most extensive cytotoxic properties of A β are mediated by smaller less ordered assemblies of A β [4,11,12]. Accordingly, A β aggregation-based strategies to search for AD-modifying drugs should be targeted to prevent buildup of any toxic oligomeric species along the assembly reaction.

One approach to inhibit an aggregation reaction is to re-design the self-recognition interface of peptide or protein molecules, in a manner that the modified molecule is still capable of interacting with the native form, but inhibits its further assembly into larger aggregates [13]. This approach was successfully exploited for example in the case of Islet Amyloid Polypeptide (IAPP) [13,14]. IAPP is a hydrophobic strongly amyloidogenic peptide, which is produced in the pancreatic islet cells and plays, in the soluble monomeric form, a major role in glucose homeostasis [15]. In certain circumstances, this peptide undergoes a transition from a predominantly random coil monomeric state to β -sheet aggregates, and these aggregates have been shown to be strongly toxic for several cell types and associated with the progressive destruction of pancreatic beta cells in adult-onset diabetes [16]. To keep the physiologic function of IAPP but block its amyloid forming propensity, an IAPP analogue was designed through the structure-based introduction of a minimum number of two N-methyl groups, at Gly24 and Ile26, located in the amyloid core and with side chains presumably pointing into a similar direction (see Figure 1A) [13,17]. It was shown that the so-called IAPP-GI peptide efficiently inhibits IAPP amyloid formation and cytotoxicity [13,17]. More interestingly, IAPP-GI was demonstrated to block cytotoxic assembly of A β and insulin as well [18,19]. The cross-association reaction between IAPP-GI (or nonfibrillar IAPP conformers) and A β may have some implications beyond its

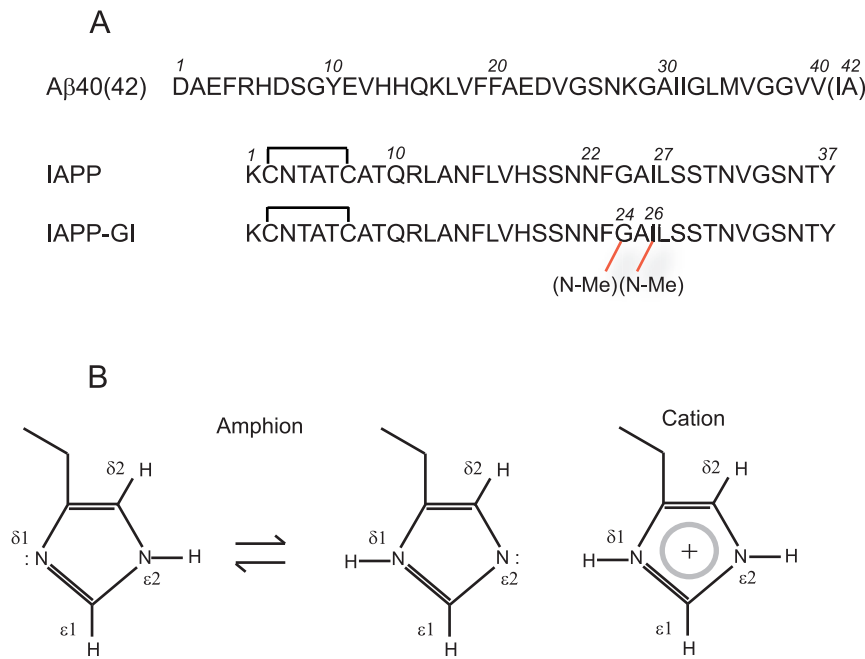


Figure 1. Primary structures of Aβ, IAPP and IAPP-GI (A) and tautomeric and protonation states of histidine side chain (B). ^1H - ^{15}N HSQC spectra of histidine side chains were acquired with coherence transfer from $\epsilon 1\text{H}$ and $\delta 2\text{H}$ to $\epsilon 2\text{N}$ and $\delta 1\text{N}$ through ^2J coupling constants. doi:10.1371/journal.pone.0020289.g001

therapeutic potentials, and along with clinical and epidemiological evidences, provide a potential molecular link between AD and adult-onset diabetes [20]. On a more general level and based on recent evidence for other cross-interactions between amyloidogenic polypeptides and proteins including the Aβ-tau and the Aβ-prion protein interaction, it appears that cross-amyloid interactions may play a critical role in neurodegenerative diseases [21,22].

In the current study, we make use of solution Nuclear Magnetic Resonance (NMR) measurements to investigate the intermolecular interaction of Aβ with IAPP-GI. Considering the high sequence similarity of Aβ and IAPP-GI and the blockade of Aβ aggregation by IAPP-GI, the results of this study may assist in understanding the mechanism of the very early steps of Aβ self-association into cytotoxic aggregates and fibrils and its inhibition.

Results and Discussion

Both Aβ and IAPP peptides show a remarkable hydrophobicity in the sequence and a high tendency to self-associate, especially at concentrations which are normally used in NMR experiments. Accordingly, Aβ-IAPP hetero-association may encounter significant kinetic and/or thermodynamic barriers if peptide self-association is a competing alternative scenario for them. Therefore, we needed to find an experimental condition under which these two peptides predominantly populate a monomeric state. Several studies demonstrate that the full-length Aβ40 is mostly monomeric at neutral pH [8,23], and the peptide does not significantly change the assembly state if the sample is stored at concentrations below 100 μM and temperatures as low as 5°C, provided that the sample is devoid of preformed aggregates [8]. IAPP is also known to be much less prone to aggregation at lower temperatures [24], and it has been suggested on the basis of analytical ultracentrifugation and diffusion NMR spectroscopy that human IAPP is in a kinetically stable state consisting of

monomers and high molecular weight oligomers at neutral pH and 4°C, even at a concentration as high as 255 μM (1 mg/mL) [24,25]. However, at temperatures above 20°C, the strong self-association propensity of human IAPP rapidly drives monomeric IAPP molecules toward oligo- and multimerization [24–27]. At this temperature, IAPP-GI has also been shown to self-associate - similarly to IAPP- with low nanomolar affinity into soluble di- and oligomers [13]. In contrast to IAPP, however, IAPP-GI oligomers were found to be unable to further aggregate into cytotoxic aggregates and amyloid fibrils, due to the conformational constraint imposed by the two N-methylations [13,17]. Taking all these points into consideration, we selected as our titration experimental condition a low temperature of 5°C and a neutral pH of 7.3 buffered with 20 mM sodium phosphate without addition of any salt. Aβ40, Aβ42 - that shows a higher aggregation propensity than Aβ40 and is believed to be the primary toxic amyloid β peptide [2] - and IAPP-GI in their lyophilized states were dissolved in 10 mM NaOH and pure HFIP, respectively, as recommended in references [8,15]. Aβ concentrations were kept constant at 30 μM along the titration experiment, while the IAPP-GI concentration was varied in the range of 0–480 μM [25].

The 1D ^1H -NMR spectra of Aβ40 and Aβ42 in the absence of IAPP-GI are characteristic of unfolded peptides, i.e. methyl resonances are found in two narrow regions of 0.8–1 and 1.3–1.4 ppm, characteristic for random coil shifts of Val, Leu, Ile and Ala (Figures 2 and S1). In agreement with the absence of a threonine residue in the Aβ40 as well as Aβ42 primary sequence, no signal was observed at around 1.1 ppm. After addition of IAPP-GI, the overall signal intensity was increased, and some new signals appeared, e.g. there were two new signals at around 1.1 and 1.2 ppm, i.e. close to the random coil chemical shift of the methyl group of Thr residues, and therefore probably originate from the four Thr residues of IAPP-GI. In addition, NMR signals were observed at 6.82, 7.00 and 7.35 ppm exclusively in the presence of IAPP-GI (Figures 2 and S1). The intensities of the

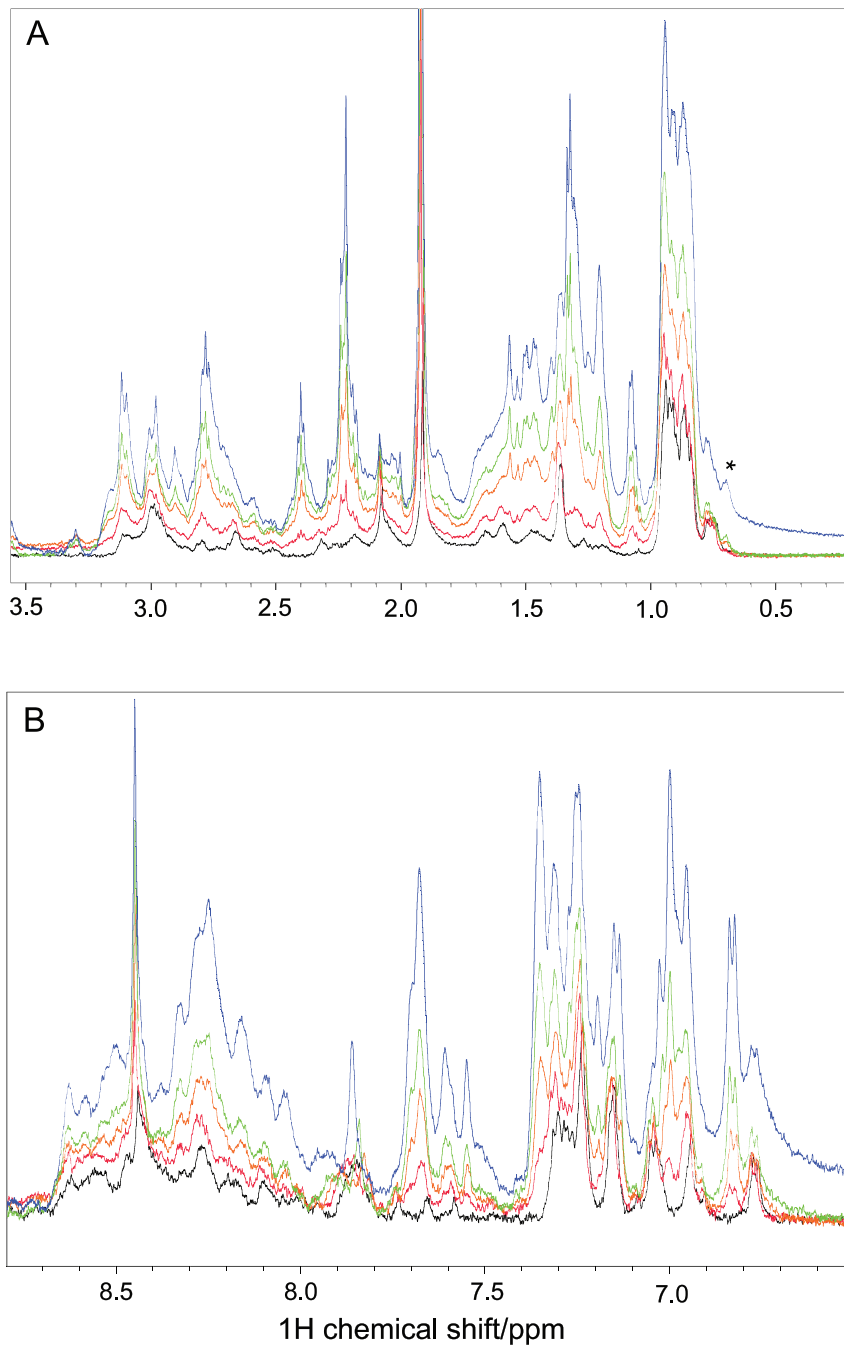


Figure 2. 1D ^1H NMR spectra of $\text{A}\beta_{40}$ with or without IAPP-GI. The aliphatic and amide regions of the spectra are shown in (A) and (B), respectively. The spectra were measured in the presence of 0 (black), 2 (red), 4 (orange), 8 (green) and 16 (blue) molar excess of IAPP-GI. Chemical shifts were calibrated on the basis of an external DSS reference and temperature was 5°C . Note the peak at 0.7 ppm, marked as *, which is probably related to an oligomeric state of IAPP-GI or $\text{A}\beta_{40}$. Peaks at 1.15, 6.82, 7.00 and 7.35 ppm are exclusively observed after addition of IAPP-GI. doi:10.1371/journal.pone.0020289.g002

IAPP-GI specific NMR signals represent sensitive probes of the concentration for the NMR-visible IAPP-GI molecules during the titration. In case of $\text{A}\beta_{40}$, the IAPP-GI specific signals increased in intensity by factors of 2.1, 3.6 and 6.8 in the spectra with 4, 8 and 16 molar excess of IAPP-GI when compared to the spectrum with two-fold excess of IAPP-GI. The slower rise in the peak intensity than expected on the basis of the added amount of IAPP-GI suggests that IAPP-GI partially aggregates to large NMR-invisible states during the titration. In case of $\text{A}\beta_{42}$, the relative intensity of

the IAPP-GI specific NMR signals increased even less with increasing IAPP-GI concentration, suggesting that the $\text{A}\beta$ peptide and its specific aggregation propensity plays a role in aggregation of IAPP-GI (Figure S1). The formation of aggregates during the titration is further supported by the emergence of an additional, relatively broad signal at around 0.7 ppm (marked with *), which appeared at a IAPP-GI: $\text{A}\beta_{40}$ ratio of 4:1 and became stronger at the ratio of 16:1. In case of $\text{A}\beta_{42}$, this broad peak is already present at a IAPP-GI: $\text{A}\beta_{42}$ ratio of 1:1. The new NMR signal may

be related to an oligomeric state of IAPP-GI in co-existence with the monomeric state, as suggested for IAPP at low temperatures [25], or alternatively be caused by an oligomeric state of A β , now induced by a high concentration of IAPP-GI [28].

To obtain site-resolved information about the interaction of A β with IAPP-GI, a series of two-dimensional ^1H - ^{15}N HSQC measurements were performed for 30 μM of ^{15}N -labeled A β 40 and A β 42 at increasing concentrations of IAPP-GI. Increasing concentrations of IAPP-GI resulted in a uniform reduction of signal intensities of A β 40 and A β 42: the average intensity ratio of the backbone signals of A β 42 was $0.57(\pm 0.02)$ for the last titration point when compared to the first one (Figures 3A and S2). In addition, the side-chain signals of Arg5, Gln15 and Asn27 obeyed a similar trend of decreasing intensity. The uniform loss of NMR signal intensities in the backbone and side chains upon increasing IAPP-GI concentrations suggests that IAPP-GI induces aggregation of A β 42 into large oligomeric NMR-invisible states. The bigger loss of A β 42 intensity when compared to A β 40 (43 percent *vs* 16 percent at the same IAPP-GI/A β ratio) is consistent with the higher aggregation propensity of A β 42 compared to A β 40. Together with the aggregation of IAPP-GI in the presence of A β described above (Figures 2 and S1), our data reveal a concentration-dependent co-aggregation of A β and IAPP-GI that is enhanced for the more aggregation prone A β 42 peptide.

Besides the uniform decrease in NMR signal intensity, several residues showed small changes in their N and H^{N} chemical shifts after addition of IAPP-GI, while no significant chemical shift perturbation was found in the control experiments (Figure 3B). The strongest chemical shift changes were observed in a stretch of the peptide extending from His13 to Phe20, with additional perturbations appearing at residues Arg5, Ser8 and Asp23 (Figure 4A). Moreover, chemical shift changes of most of the peaks followed a linear relationship up to a molar ratio of IAPP-GI:A β 40 of 16:1, with the largest linear slopes observed for residues His13-Lys16 (Figure 4B). Similar chemical shift changes were observed upon addition of IAPP-GI to A β 42 (Figure 5). The gradual change in chemical shifts, the absence of new peaks and the lack of any site-specific broadening effect during the titration, suggests that the interaction between the two peptides occurs in the fast exchange regime on the NMR time scale and that the affinity of IAPP-GI to bind A β is relatively weak at the conditions of the NMR experiment.

At first sight, the low affinity between A β and IAPP-GI observed in the NMR experiments appears to be in contrast with the previously reported affinity of their interaction as derived from fluorescence titration assays [18]. In these studies, N-terminal fluorescein labeled IAPP-GI (Fluos-IAPP-GI) (1 nM) was titrated with A β 40 using low nano- to submicromolar A β 40 concentrations and an app. K_{d} of 50 nM was determined [18]. Our current results together with those of previous studies suggest, however, that the differences in apparent affinities are due to different peptide assembly states - regarding both A β 40 and IAPP-GI - present in the NMR titration studies as compared to the fluorescence titration assay [18]. Indeed, at the micromolar peptide concentrations used in the NMR titration study, two oligomeric A β 40 species of ~ 30 and ~ 150 nm in hydrodynamic radius were observed using dynamic light scattering (Figure S3 and Methods S1), despite using NaOH to dissolve pre-formed A β 40 aggregates [8]. Addition of IAPP-GI led then to further aggregation of A β 40 as shown above. Similar to A β 40, IAPP-GI populates an aggregate state in equilibrium with the monomeric state, with a shift toward aggregation occurring at higher IAPP-GI concentrations [26]. In fact, the high self-assembly propensity of IAPP-GI into soluble but -in contrast to IAPP- nonamyloidogenic

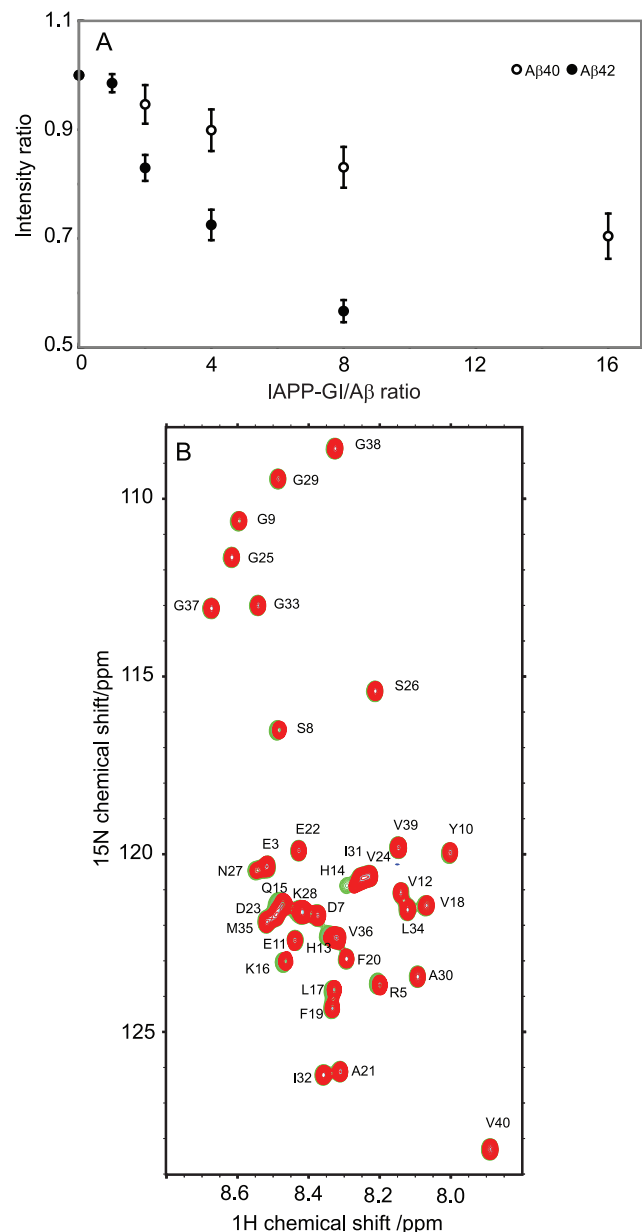


Figure 3. Probing the binding of IAPP-GI to A β using NMR spectroscopy. A. Variation of ^1H - ^{15}N -HSQC peak intensity of A β 40 or A β 42 upon titration with un-labeled IAPP-GI. Intensity ratios were calculated relative to intensities of free A β spectra, and error bars represent variation along the sequence. Note that loss of signal intensity is more enhanced for A β 42 than A β 40. B. ^1H - ^{15}N -HSQC spectra of A β 40 in the absence (green) or presence of 16 molar excess of non-labeled IAPP-GI (red). A shift in the position of His13, His14, Gln15, Lys16 and Leu17 peaks is evident.
doi:10.1371/journal.pone.0020289.g003

dimers and oligomers, with self-assembly starting already in the low nanomolar concentration range, has been earlier demonstrated using various biophysical methods [13]. These included fluorescence spectroscopy, i.e. titration of Fluos-IAPP-GI (1 nM) with IAPP-GI (app. K_{d} , 4 nM) [13], transmission electron microscopy [13], CD concentration dependence studies ([13], see also Figure S4 and Methods S1), size exclusion chromatography [13], and SDS-PAGE and Western blot analysis of cross-linked IAPP-GI samples [18]. Based on the above data, it becomes

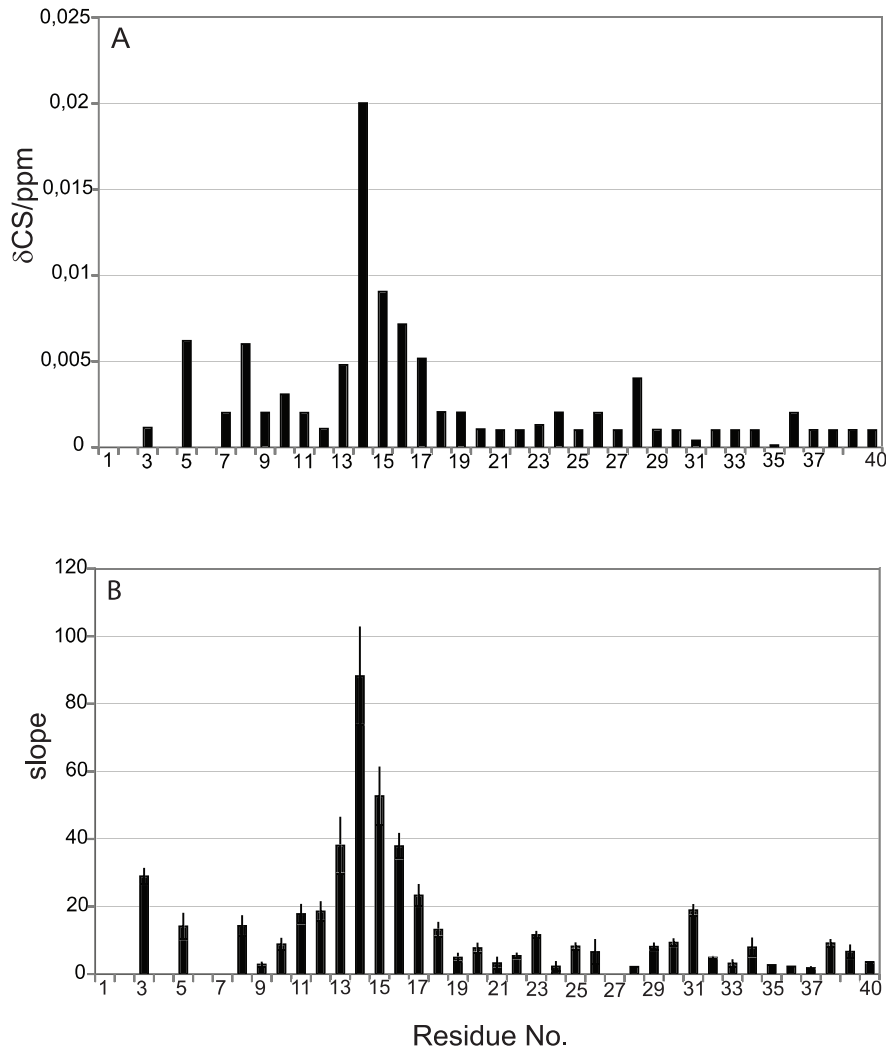


Figure 4. NMR chemical shift perturbation in A β 40 upon addition of IAPP-GI. A. Average backbone N and H^N chemical shift difference of A β 40 after addition of a 16 fold molar excess of IAPP-GI. B. Slope of the best fitted line to chemical shift perturbation vs IAPP-GI concentration data, presented in units of ppm/M. doi:10.1371/journal.pone.0020289.g004

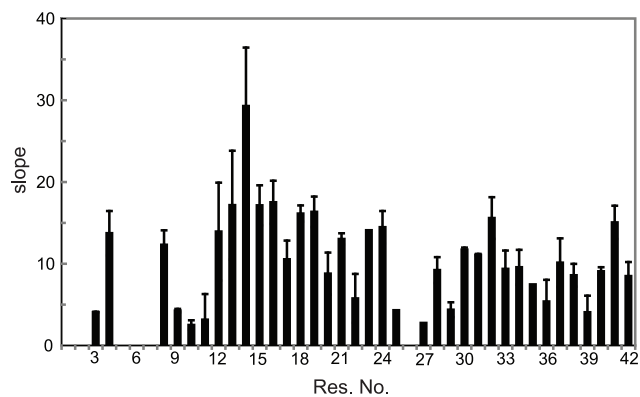


Figure 5. Average backbone N and H^N chemical shift perturbation in A β 42 upon addition of IAPP-GI. The values are reported as slope of the best fitted line to chemical shift difference vs IAPP-GI concentration data, in units of ppm/M. doi:10.1371/journal.pone.0020289.g005

evident that while the app. K_d of the IAPP-GI-A β 40 interaction measured using fluorescence spectroscopy was determined under conditions where IAPP-GI is mainly in a monomeric state [13] and A β 40 mainly in a monomer or dimer state (submicromolar concentrations), the interaction followed in our NMR study here included at least in a large part interactions between (NMR-visible) A β monomers and IAPP-GI oligomeric assemblies. Therefore, the actual monomeric concentrations of A β and IAPP-GI under the NMR conditions were considerably less than the nominal peptide concentrations, and the apparent affinities observed here using NMR are not comparable with those of fluorescence titration assays obtained at nanomolar concentrations of A β 40 and IAPP-GI. In addition, as both IAPP-GI and A β 40 (or A β 42) have been recently shown to use the same regions in their self- and hetero-association processes, a reduced affinity between interactions of their oligomeric states would be expected which is consistent with the NMR observations [38]. At the same time, however, a strong inhibitory effect of IAPP-GI on A β 40 and A β 42 fibrillogenesis and cytotoxicity has been shown using assay systems containing low micromolar concentrations of A β and IAPP-GI [18,38], suggesting

that our studies are relevant for the understanding of the inhibitory mechanism of IAPP-GI on A β . To obtain more direct evidence for the effect of IAPP-GI oligomerization on its binding affinity to A β 40, we titrated synthetic N-terminal fluorescein labeled A β 40 (Fluos-A β 40) (1 nM) with increasing amounts of IAPP-GI (Figure S5 and Methods S1). Binding of IAPP-GI to Fluos-A β 40 resulted in a strong increase of the fluorescence emission. A sigmoidal binding isotherm was obtained with a plateau at an IAPP-GI concentration between 250–500 nM and curve fitting yielded an app. K_d of 39 nM for the Fluos-A β 40-IAPP-GI interaction of 39 nM (Figure S5A). The obtained K_d was nearly identical to the app. K_d of 41.2 nM (\pm 3.9) which was obtained by titrating Fluos-IAPP-GI (1 nM) with A β 40 confirming thus this previously reported high affinity of interaction between the two peptides [18]. However, titrating Fluos-A β 40 with IAPP-GI using IAPP-GI concentrations higher than 500 nM, i.e. between 1–10 μ M, resulted in a dramatic decrease of the fluorescence emission determined at the plateau of the Fluos-A β 40-IAPP-GI mixture (Figure S5B). These findings were consistent with the suggestions (a) that significant amounts of different IAPP-GI oligomeric assemblies are populated at concentrations higher than 1 μ M as compared to the species present between 1 and 500 nM and (b) that formation of the above IAPP-GI oligomers likely depletes from the solution large amounts of the IAPP-GI species which are able to bind A β 40 with low nanomolar affinity.

To obtain further insights into the contribution of His13 and His14 for binding to IAPP-GI, side chain ^1H - ^{15}N HSQC spectra in the free and IAPP-GI-interacting forms of A β 40 were compared. The chemical shifts of the ϵ 2 and δ 1 nitrogens of the imidazole ring of histidine residues and their pattern of coupling to carbon-attached ϵ 1 and δ 2 protons are sensitive probes of their protonation, tautomeric and hydrogen bonding states [29]. As depicted in Figure 6, peaks of all three histidine side chains (including His6, which is not present in the backbone spectra) could be observed, and two of them, probably the consecutive His13 and His14, have very similar chemical shifts of ϵ 2N, δ 1N and ϵ 1H. There is a large dispersion in the nitrogen dimension, indicating that the imidazole ring should be in an amphionic (non-protonated) state. This is consistent with the pH 7.3 of our sample, which is around one unit above the expected pKa of histidines. The chemical shifts of the ϵ 2 and δ 1 nitrogens are in the range of 177–180 and 218–220 ppm, respectively, suggesting that they may be involved in some form of H-bonds [30]. The observed pattern of coupling of ^{15}N nuclei to ^1H denote that the histidine side chains are largely populated in a tautomeric state in which ϵ 2N is attached to a proton, and the weak intensity of the δ 2H- δ 1N peak suggest a small but still detectable ^3J coupling between them [31]. After addition of IAPP-GI, the large dispersion in ^{15}N dimension and the characteristic pattern of coupling between ^{15}N and ^1H nuclei remained unchanged. However, the following changes were observed: first, while all three ϵ 2N chemical shifts were changed by a similar value of 0.8 ppm toward downfield, δ 1N chemical shifts were affected more strongly and not in a uniform manner. The perturbation of the δ 1N chemical shift was 4.7 and 6.5 ppm for two histidines and around 10 ppm for the third one, which is also severely broadened. Secondly, all the peaks experienced a significant degree of broadening upon addition of IAPP-GI. The intensity ratio for the ϵ 2N correlations was between 20 and 30% for all the histidines of A β 40. In contrast, for the δ 1N correlations, it was 28 percent for one and only about 7 percent for the other two. Third, the weak ^3J -based δ 1N- δ 2H peaks completely disappeared after addition of IAPP-GI. The direction of chemical shift deviation can be taken to suggest that, after interaction with IAPP-GI, δ 1N of His13 and His14 spends more time in the

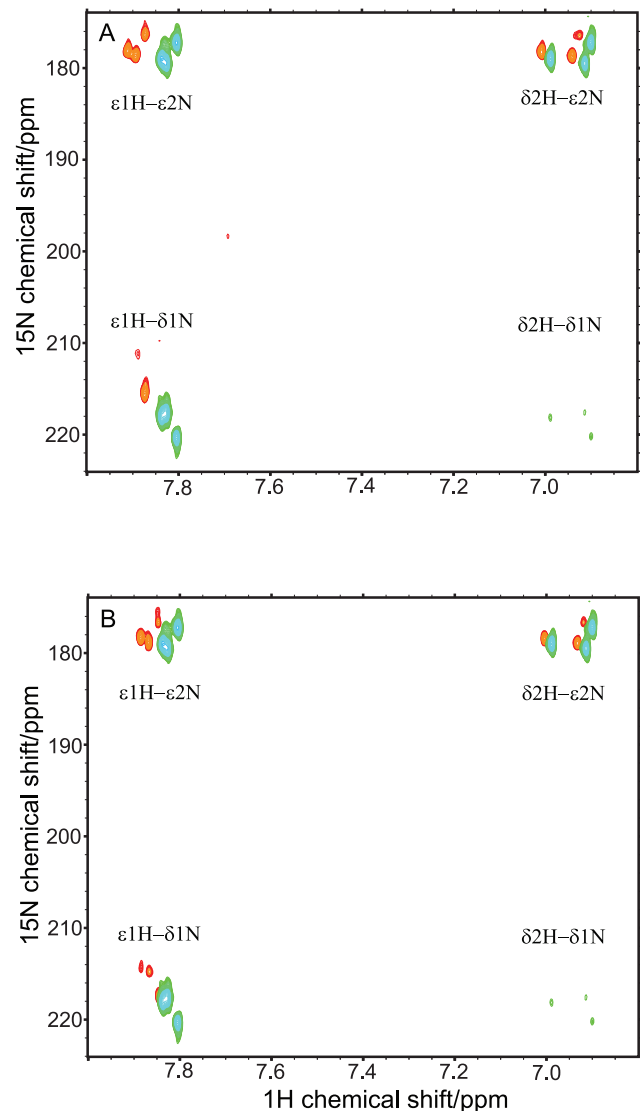


Figure 6. Influence of IAPP-GI binding on the protonation and tautomeric states of the histidines. A. Side chain ^1H - ^{15}N -HSQC spectra of A β 40, in the absence (green) and presence (red) of IAPP-GI. Magnetization was transferred through an INEPT-based coherence transfer from ϵ 1 and δ 2 protons of histidine side chains to ϵ 2 and δ 1 nitrogen nuclei (see Figure 1B). The total duration of the INEPT was set to 27.8 ms. B. Comparison of side chain ^1H - ^{15}N -HSQC spectra of A β 40 (green) and A β 42 (red). The cross-peak pattern of all the three histidine residues of A β (His6, His13 and His14) was observed. doi:10.1371/journal.pone.0020289.g006

protonated state and/or by average, has a smaller degree of solvent exposure [30]. The change in the protonation state cannot be caused by a variation of the sample pH, as the pH was accurately adjusted after addition of IAPP-GI. Instead, it is likely to originate from a change in the pKa of the histidines caused by binding-induced changes in the micro-environment. The significant broadening of the δ 1N correlations might be attributed to a fast/intermediate exchange of A β 40 between free and bound forms. To further investigate if these changes are caused by intermolecular interactions between A β 40 and IAPP-GI, we measured the same spectra for the more aggregation-prone A β 42. As displayed in Figure 6B, pure A β 42 showed a pattern that is very similar to that of A β 40 with IAPP-GI, further

suggesting that the observed changes could be an effect of transient intermolecular interactions between A β and IAPP-GI.

Next, we measured sequence specific water-amide proton exchange rates for A β 40 in the absence and presence of IAPP-GI using CLEANEX-PM-FHSQC experiments [32]. The water-amide proton exchange rate is a valuable probe of the degree of exposure of the protein backbone to the solvent: a N-H group that is buried inside the protein or involved in a hydrogen bond, will be protected from exchange with solvent. In a CLEANEX-PM-FHSQC experiment, exposed parts of the backbone gain high signal intensity already at short mixing times due to efficient exchange with water, while for more protected groups the signal intensity only rises at longer mixing times. In the absence of IAPP-GI, Gly25, Ser26, Asn27, Lys28 and Gly29 of A β 40 showed a strong increase in NMR signal intensity already at a mixing time of 100 ms (Figure 7). The solvent exposure of these residues was further corroborated by analysis of the initial exchange rate

(Figure 8A): the highest exchange rates were observed for residues Ser8-Gly9, His14, Lys16, Asp23, Gly25-Gly29 and Gly37-Gly38. Interestingly, Gln15-Val24 and Ala30-Val36 have a high tendency to adopt α -helical [33] or β -strand [34] secondary structures, while the intervening region of Val24-Gly29 tends to form a loop [35]. Additionally, solid-state NMR studies of A β fibrils have verified that the region between residues 23 and 29 forms an exposed turn-like structure between two β -strands [36,37]. Altogether, the observed profile of exchange rates suggests that the monomeric free form of A β 40 transiently samples conformational states, in which residues 10-13, 17-22 and 30-36 are partially protected from exchange with solvent. Addition of IAPP-GI results in a decrease of the exchange rate of residues Asp7, Gly9, Gln15 and Lys16, as well as Val24-Val36 (Figure 8B). The reduced exchange rates suggest that these residues are less exposed to the solvent after IAPP-GI addition. Increased protection could be a result of an intermolecular interaction between IAPP-GI and A β 40, or

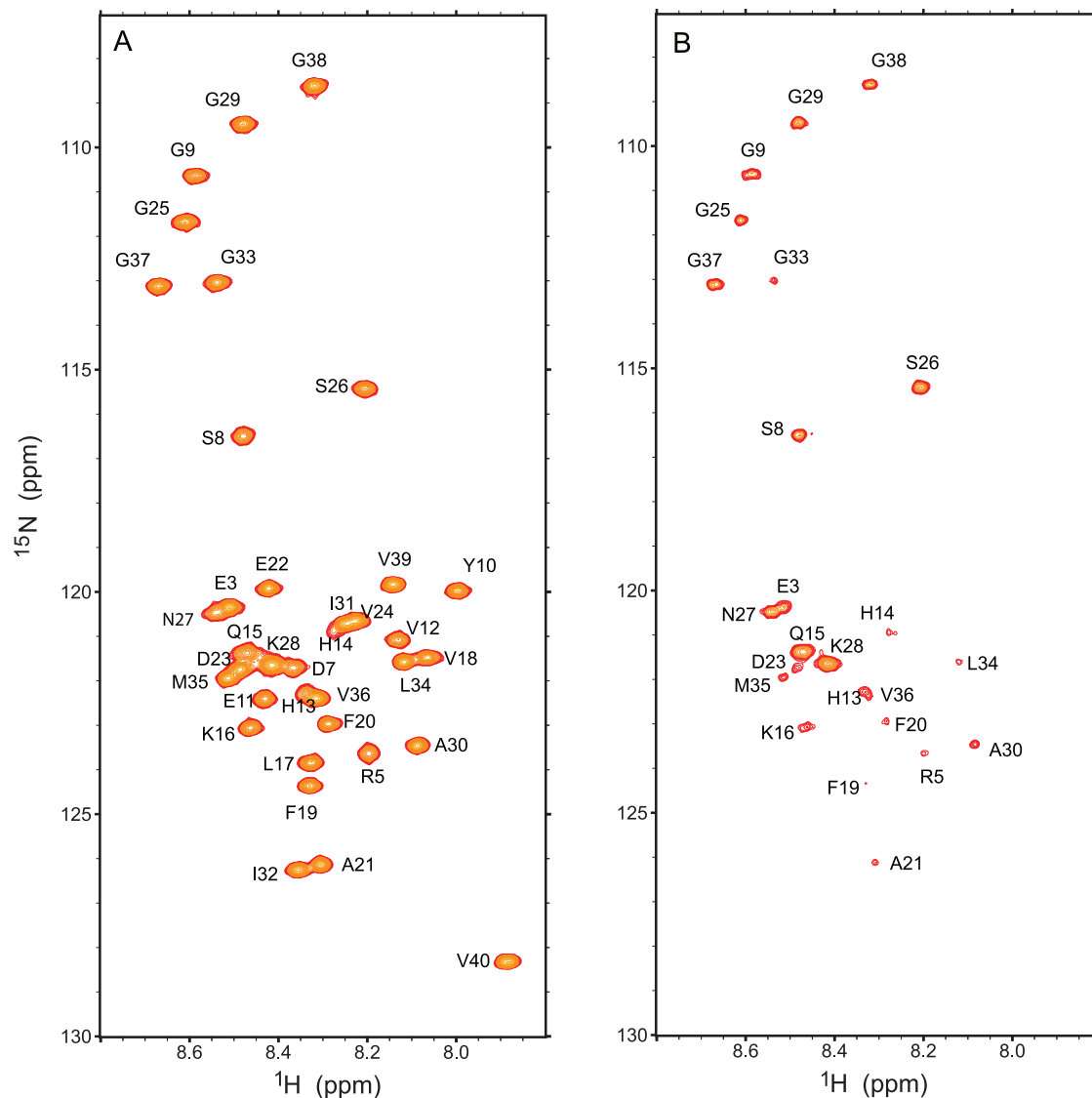


Figure 7. Probing the water-amide proton exchange rates through a CLEANEX-PM-FHSQC experiment. A. ^1H - ^{15}N -FHSQC spectrum of free A β 40. The peak intensities of the ^1H - ^{15}N -FHSQC spectrum were used as reference to calculate the relative intensity of peaks due to chemical exchange. B. CLEANEX-PM-FHSQC spectrum, measured after a selective excitation of water protons and a following 100 ms mixing time during which chemical exchange between water and amide protons occurred variably for different residues of A β 40. doi:10.1371/journal.pone.0020289.g007

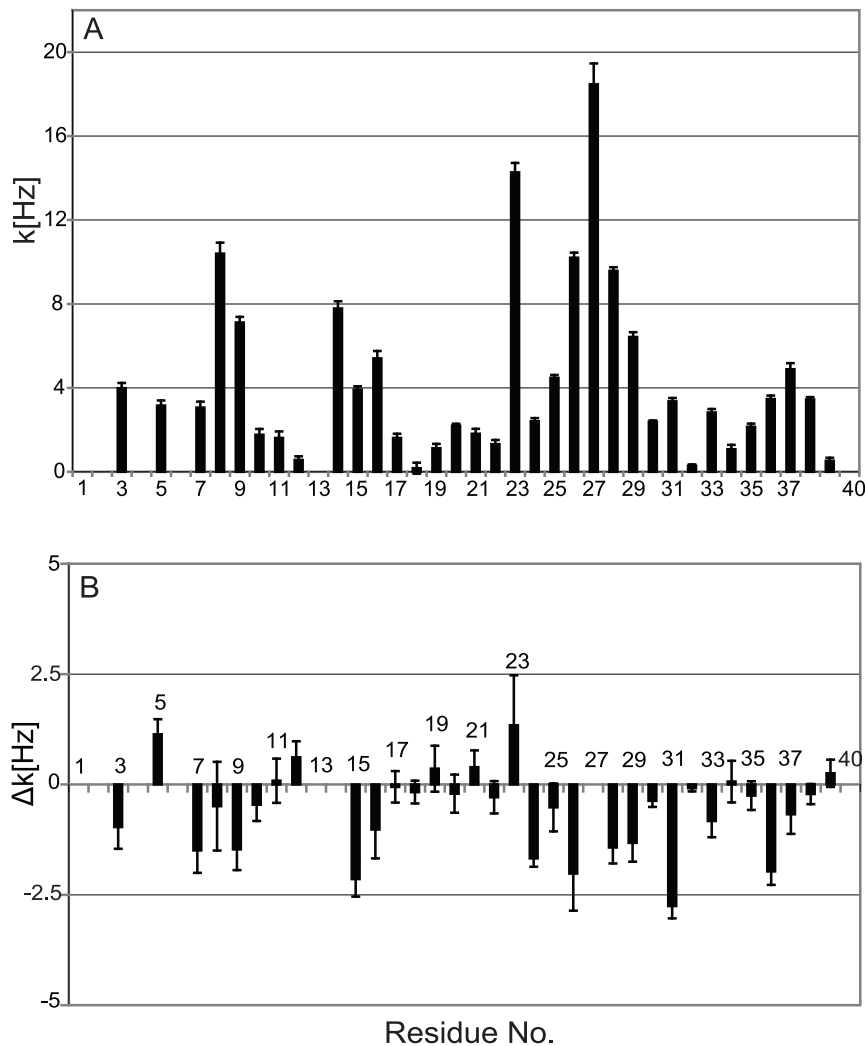


Figure 8. Initial water-amide proton exchange rates (k). A. Exchange rate, k , along the sequence of A β 40 in the free form, measured through a CLEANEX-PM-FHSQC experiment. B. The change in exchange rate of A β 40 residues after addition of a 16-molar excess of IAPP-GI. Residue numbers are indicated.

doi:10.1371/journal.pone.0020289.g008

alternatively caused by an IAPP-GI induced change in the conformation or assembly state of A β 40. Support for the influence of intermolecular interactions comes from a comparison of exchange rates in A β 40 and A β 42. In A β 42, which has a higher tendency for self-association, the exchange rates are reduced in regions (Figure 9) that are also affected upon addition of IAPP-GI to A β 40 (Figure 8B).

A recent analysis of the A β -IAPP and A β -IAPP-GI interaction interface using synthetic peptides and peptide arrays has shown that the “hot spot regions” of the A β -IAPP and A β -IAPP-GI interfaces are localized predominantly within the two regions which are converted into β -strands in amyloid fibrils [38]. These studies have also suggested that the hydrophobic C-terminal part of A β (residues 29–40) binds IAPP (and IAPP-GI) with a 10-fold higher affinity as compared to the N-terminal part (residues 1–28), which binds IAPP with low μ M affinity [38], and that the region between Phe19 and Glu22 was the shortest residue stretch in the N-terminal part of A β required for low μ M binding, while no evidence for a direct interaction of the A β region between His13 and Leu17 was observed [38]. Our NMR chemical shift perturbation data assign now an important role in the A β -

IAPP-GI interaction to residues His13 to Leu17, the region of A β that is important for binding to ganglioside micelles [39]. At the same time, the water-amide proton exchange data of A β 40 in the absence and presence of IAPP-GI suggest that in addition to the N-terminal region, residues in the C-terminal part are also involved in the interaction. Taking all these findings into consideration, we propose the following model for the A β 40-IAPP-GI interaction: The C-terminal part of A β is directly involved in intermolecular interaction with IAPP-GI. This intermolecular interaction induces a conformational change in the N-terminal part of A β , which is favored by the high propensity of the N-terminal region of A β 40 to assume secondary structure [33,34]. The conformational transition then leads to changes in pK_a and protonation state of the histidine residues. Since the IAPP-GI peptide has a high degree of sequence similarity to A β , the A β -IAPP-GI interaction might represent some of the initial steps in self-association of A β molecules. In fact, the proposed model for interaction between A β and IAPP-GI has some similarities with a recently published structure of A β oligomers, where the N- and C-terminal parts of A β are involved in intra- and inter-molecular interactions, respectively [40].

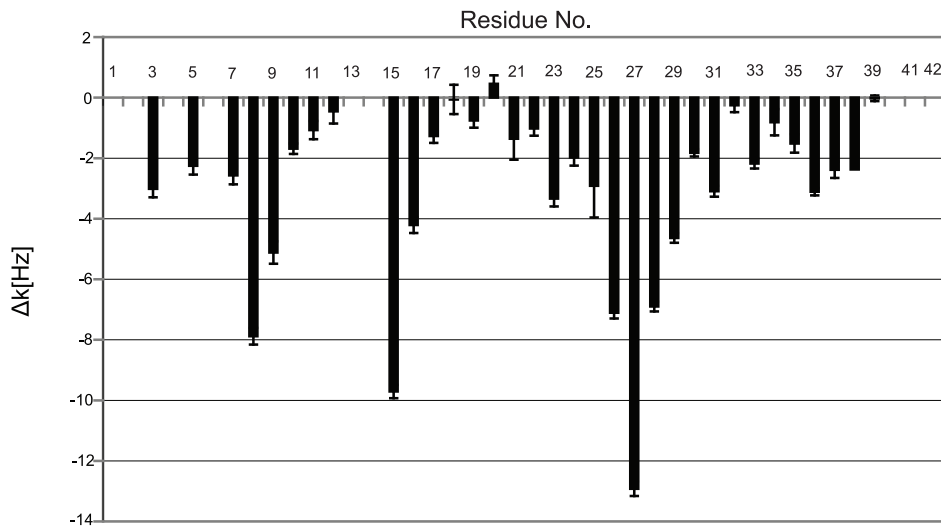


Figure 9. Difference between the initial water-amide proton exchange rates of A β 42 and A β 40 ($\Delta k = A\beta_{42} - A\beta_{40}$). The initial exchange rates were measured through a CLEANEX-PM-FHSQC experiment. Most residues show less solvent exposure in A β 42 than A β 40. doi:10.1371/journal.pone.0020289.g009

The prominent loss of NMR signal intensities in the ^1H - ^{15}N HSQC spectra of A β 40 and A β 42 upon increasing concentrations of IAPP-GI points to a IAPP-GI dependent conversion of A β to an NMR-invisible state, i.e. a large and/or non-homogeneous aggregate state with slow tumbling and/or significant inhomogeneity that broaden its signals beyond experimental detection level. Because the NMR-visible signals of IAPP-GI are reduced at the same time, it is most likely that aggregates are formed that comprise both A β and IAPP-GI [18]. In agreement with their intrinsic aggregation propensities, the aggregation is more evident in the case of A β 42 than A β 40. As it has previously been shown that IAPP-GI significantly lowers A β -mediated toxicity when both are mixed in micromolar concentrations, i.e. similar to the conditions used in the current study, our data suggests that the aggregate state of A β induced in the presence of IAPP-GI is not a toxic “on-pathway” aggregate, but a nontoxic “off-pathway” aggregate which is consistent with previous findings [18]. A similar redirection of A β and α -synuclein into off-pathway oligomers was previously reported for the polyphenol (-)-epigallocatechin gallate [41], suggesting a similar toxicity lowering mechanism of IAPP-GI and (-)-epigallocatechin gallate, at least at high inhibitor/peptide concentrations. Finally, our studies provide evidence that the interaction between A β and IAPP-GI leads to a conformational change in the region A β (13–17) that might be related to the inhibitory effect of IAPP-GI on A β “on-pathway” aggregation and cell toxicity.

Materials and Methods

Materials

^{15}N -uniformly labeled A β 1–40 and A β 1–42 was purchased from rPeptide, and dissolved in 10 mM NaOH solution at 2 mg/mL concentration [8]. Synthetic IAPP-GI was synthesized as previously described [13] and dissolved in pure 1,1,1,3,3,3-hexafluoroisopropanol (HFIP) at a concentration of 5 mg/mL. N-terminal fluorescein labeled A β 40 was prepared as described for the labeled IAPP segments [38]. HFIP was obtained from Fluka. Before titration experiments, the solvent (HFIP) was evaporated under N_2 gas and phosphate buffer was used to dissolve dried IAPP-GI.

NMR Spectroscopy

All NMR spectra were recorded at 278 K with a sample of 30 μM ^{15}N -uniformly labeled A β 40 or A β 42, with or without the specified concentration of non-labeled IAPP-GI, in 20 mM sodium phosphate buffer at pH 7.3 (adjusted after adding peptides). Chemical shift referencing at this temperature was made with respect to the external 4,4-dimethyl-4-silapentane-1-sulfonic acid (0.0 ppm). All NMR spectra were processed and analyzed with NMRPipe and Sparky.

The interaction of IAPP-GI with A β 40 and A β 42 was assessed through a series of ^1H - ^{15}N HSQC spectra of A β in the presence of 0, 2, 4, 8 and 16 molar excess of IAPP-GI for A β 40 and 0, 1, 2, 4 and 8 molar excess of IAPP-GI for A β 42. Titrations were made on the same peptide sample, and temporal stability of peptide solutions were checked with 1D ^1H -NMR spectra measured before and after each NMR experiment. The spectra were measured on a Bruker Avance 600 MHz spectrometer equipped with a triple-resonance room temperature probe. The time domain data contained 1 K and 220 complex data points in t_2 and t_1 , respectively. The 90° -shifted squared sine bell function was used as apodization function in both dimensions, yielding a final matrix of $8\text{K} \times 512$ data points. The peak assignments were obtained from the literature, and their deviation from the original position was monitored as a function of IAPP-GI/A β molar ratio. The average chemical shift deviation was calculated as the root square of $(\Delta N/5)^2 + (\Delta H)^2$, where ΔN and ΔH were the chemical shift difference of N and H^{N} resonances compared to the control experiment. The first (IAPP-GI:A β ratio of 0) and last (IAPP-GI:A β ratio of 16) experiments were re-measured on the higher field Bruker AMX 800 MHz, equipped with a cryogenic probe to confirm the observed chemical shift perturbations. In a control experiment, A β 40 was similarly titrated with phosphate buffer after dissolving the dried HFIP (without IAPP-GI) under N_2 gas.

^1H - ^{15}N HSQC spectra of the side chains of histidines (H6, H13 and H14) were acquired on a Bruker AMX 600 MHz spectrometer equipped with a triple-resonance cryogenic probe. The sample was 30 μM A β 40, with or without a 16 molar excess of IAPP-GI. A 30 μM sample of A β 42 was also measured. The INEPT transfer delay was selected as 27.8 ms, to obtain the coherence transfer from the $\epsilon_1\text{H}$ and $\delta_2\text{H}$ protons to the $\epsilon_2\text{N}$ and

$\delta 1\text{N}$ through the ^2J coupling constant (Figure 1B). The carrier and SWH values were 5.00 ppm and 6010 Hz in the direct dimension, and 185.31 ppm and 9728 Hz in the indirect dimension. The experimental matrix was $2\text{K} \times 256$ complex data points, which after apodization through a 90° -shifted squared sine bell function in both dimensions was transformed to a final matrix of $8\text{K} \times 512$ data points.

The solvent accessibility of the A β 40 backbone in the free and possibly IAPP-GI-bound forms was evaluated through measurement of exchange rates between water and NH protons. To this end, CLEANEX-PM-FHSQC experiments were recorded on a Bruker Avance 600 MHz spectrometer equipped with a triple-resonance room temperature probe. In a CLEANEX-PM-FHSQC experiment, a selective water excitation is followed by a mixing time (τ_m) of durations 4, 8, 16, 24, 32, 48, 75, 100, 200 and 500 ms, during which chemical exchange between water and NH protons takes place. The intensity of peaks as a function of mixing time was fitted to the following equation:

$$V/V_0 = k \cdot \{\exp(-R_{1B} \cdot \tau_m) - \exp[-(R_{1A} + k) \cdot \tau_m]\} / (R_{1A} + k - R_{1B}) \quad (1)$$

where V_0 is the intensity of the peak in a control FHSQC experiment, k is the normalized rate constant related to the forward exchange rate constant between water and NH protons, and R_{1A} and R_{1B} are apparent longitudinal relaxation rates for protein and water [32].

Supporting Information

Figure S1 1D ^1H NMR spectra of A β 42 with or without IAPP-GI. The methyl and aromatic regions of the spectra are shown in (A) and (B), respectively. The spectra were measured in the presence of 0 (black), 1 (red), 2 (orange), 4 (green) and 8 (blue) molar excess of IAPP-GI. Chemical shifts were calibrated on the basis of an external DSS reference and the temperature was set to 5°C . Peaks marked as * are observed exclusively after addition of IAPP-GI, and their relative intensities are taken to follow the rise of NMR-visible IAPP-GI concentration. (EPS)

Figure S2 Loss of the peak intensities in ^1H - ^{15}N -HSQC spectra of ^{15}N -labeled A β 42 upon addition of non-labeled

IAPP-GI. IAPP-GI/A β 42 molar ratios varied between 0, 1, 2, 4 and 8, as indicated. The intensity ratios were calculated relative to the intensities of free A β 42 spectrum.

(EPS)

Figure S3 Dynamic light scattering of A β 40. In addition to a small monomeric peak around 1.6 nm, two oligomeric peaks are observed at around 30 and 150 nm. Note that the intensity of the peaks does not reflect the relative amount of each species, as large species scatter light more intensely than the small NMR-visible monomeric species at 1.6 nm.

(EPS)

Figure S4 Far-UV CD concentration dependence study of the conformation of IAPP-GI. CD spectra of IAPP-GI were measured in aqueous buffer, pH 7.4 (1% HFIP), at peptide concentrations between 500 nM and 50 μM , as indicated.

(EPS)

Figure S5 A β 40-IAPP-GI interaction as determined by fluorescence spectroscopy. N-terminal fluorescein labelled A β 40 (Fluos-A β 40) (1 nM) was titrated with increasing amounts of IAPP-GI as indicated. (A) The binding curve of Fluos-A β 40-IAPP-GI interaction obtained using concentrations of IAPP-GI between 1–500 nM is shown (fluorescence emission at 522 nm). (B) The fluorescence emissions at 522 nm of the different mixtures of Fluos-A β 40 with IAPP-GI made using concentrations of IAPP-GI between 1 nM and 10 μM are shown. Fluorescence of Fluos-A β 40 alone was subtracted.

(EPS)

Methods S1 Dynamic Light Scattering.

(DOC)

Acknowledgments

We thank Christian Griesinger for useful discussions.

Author Contributions

Conceived and designed the experiments: NR-G AK MZ. Performed the experiments: NR-G L-MY. Analyzed the data: NR-G. Contributed reagents/materials/analysis tools: EA AK. Wrote the paper: NR-G AK MZ.

References

- Chiti F, Dobson CM (2006) Protein misfolding, functional amyloid, and human disease. *Annu Rev Biochem* 75: 333–366.
- Citron M (2010) Alzheimer's disease: strategies for disease modification. *Nat Rev Drug Discov* 9: 387–398.
- Hardy J, Selkoe DJ (2002) The amyloid hypothesis of Alzheimer's disease: progress and problems on the road to therapeutics. *Science* 297: 353–356.
- Walsh DM, Selkoe DJ (2007) Abeta oligomers - a decade of discovery. *J Neurochem* 101: 1172–1184.
- Shoji M, Golde TE, Ghiso J, Cheung TT, Estus S, et al. (1992) Production of the Alzheimer amyloid beta protein by normal proteolytic processing. *Science* 258: 126–129.
- Riek R, Güntert P, Döbeli H, Wipf B, Wüthrich K (2001) NMR studies in aqueous solution fail to identify significant conformational differences between the monomeric forms of two Alzheimer peptides with widely different plaque-competence, A beta(1–40)(ox) and A beta(1–42)(ox). *Eur J Biochem* 268: 5930–5936.
- Zhang S, Iwata K, Lachenmann MJ, Peng JW, Li S, et al. (2000) The Alzheimer's peptide abeta adopts a collapsed coil structure in water. *J Struct Biol* 130: 130–141.
- Hou L, Shao H, Zhang Y, Li H, Menon NK, et al. (2004) Solution NMR studies of the A beta(1–40) and A beta(1–42) peptides establish that the Met35 oxidation state affects the mechanism of amyloid formation. *J Am Chem Soc* 126: 1992–2005.
- Kirschner DA, Inouye H, Duffy LK, Sinclair A, Lind M, et al. (1987) Synthetic peptide homologous to beta protein from Alzheimer disease forms amyloid-like fibrils in vitro. *Proc Natl Acad Sci U S A* 84: 6953–6957.
- Pike CJ, Walencewicz AJ, Glabe CG, Cotman CW (1991) In vitro aging of beta-amyloid protein causes peptide aggregation and neurotoxicity. *Brain Res* 563: 311–314.
- Lambert MP, Barlow AK, Chromy BA, Edwards C, Freed R, et al. (1998) Diffusible, nonfibrillar ligands derived from Abeta1–42 are potent central nervous system neurotoxins. *Proc Natl Acad Sci U S A* 95: 6448–6453.
- Hartley DM, Walsh DM, Ye CP, Diehl T, Vasquez S, et al. (1999) Protofibrillar intermediates of amyloid beta-protein induce acute electrophysiological changes and progressive neurotoxicity in cortical neurons. *J Neurosci* 19: 8876–8884.
- Yan LM, Tatarek-Nossol M, Velkova A, Kazantzis A, Kapurniotu A (2006) Design of a mimic of nonamyloidogenic and bioactive human islet amyloid polypeptide (IAPP) as nanomolar affinity inhibitor of IAPP cytotoxic fibrillogenesis. *Proc Natl Acad Sci U S A* 103: 2046–2051.
- Abedini A, Meng F, Raleigh DP (2007) A single-point mutation converts the highly amyloidogenic human islet amyloid polypeptide into a potent fibrillation inhibitor. *J Am Chem Soc* 129: 11300–11301.
- Schmitz O, Brock B, Rungby J (2004) Amylin agonists: a novel approach in the treatment of diabetes. *Diabetes* 53: S233–238.
- Lorenzo A, Razzaboni B, Weir GC, Yankner BA (1994) Pancreatic islet cell toxicity of amylin associated with type-2 diabetes mellitus. *Nature* 368: 756–760.

17. Kapurniotu A, Schmauder A, Tenidis K (2002) Structure-based design and study of non-amyloidogenic, double N-methylated IAPP amyloid core sequences as inhibitors of IAPP amyloid formation and cytotoxicity. *J Mol Biol* 315: 339–350.
18. Yan LM, Velkova A, Tatarek-Nossol M, Andreetto E, Kapurniotu A (2007) IAPP mimic blocks Abeta cytotoxic self-assembly: cross-suppression of amyloid toxicity of Abeta and IAPP suggests a molecular link between Alzheimer's disease and type II diabetes. *Angew Chem Int Ed Engl* 46: 1246–1252.
19. Velkova A, Tatarek-Nossol M, Andreetto E, Kapurniotu A (2008) Exploiting cross-amyloid interactions to inhibit protein aggregation but not function: nanomolar affinity inhibition of insulin aggregation by an IAPP mimic. *Angew Chem Int Ed Engl* 47: 7114–7118.
20. Nicolls MR (2004) The clinical and biological relationship between Type II diabetes mellitus and Alzheimer's disease. *Curr Alzheimer Res* 1: 47–54.
21. Guo JP, Arai T, Miklosy J, McGeer PL (2006) Abeta and tau form soluble complexes that may promote self aggregation of both into the insoluble forms observed in Alzheimer's disease. *Proc Natl Acad Sci U S A* 103: 1953–1958.
22. Laurén J, Gimbel DA, Nygaard HB, Gilbert JW, Strittmatter SM (2009) Cellular prion protein mediates impairment of synaptic plasticity by amyloid-beta oligomers. *Nature* 457: 1128–1132.
23. Tseng BP, Esler WP, Clish CB, Stimson ER, Ghilardi JR, et al. (1999) Deposition of monomeric, not oligomeric, Abeta mediates growth of Alzheimer's disease amyloid plaques in human brain preparations. *Biochemistry* 38: 10424–10431.
24. Vaiana SM, Ghirlando R, Yau WM, Eaton WA, Hofrichter J (2008) Sedimentation studies on human amylin fail to detect low-molecular-weight oligomers. *Biophys J* 94: L45–47.
25. Soong R, Brender JR, Macdonald PM, Ramamoorthy A (2009) Association of highly compact type II diabetes related islet amyloid polypeptide intermediate species at physiological temperature revealed by diffusion NMR spectroscopy. *J Am Chem Soc* 131: 7079–7085.
26. Kaye R, Bernhagen J, Greenfield N, Sweimeh K, Brunner H, et al. (1999) Conformational transitions of islet amyloid polypeptide (IAPP) in amyloid formation in vitro. *J Mol Biol* 287: 781–796.
27. Rhoades E, Agarwal J, Gafni A (2000) Aggregation of an amyloidogenic fragment of human islet amyloid polypeptide. *Biochim Biophys Acta* 1476: 230–238.
28. Narayanan S, Reif B (2005) Characterization of chemical exchange between soluble and aggregated states of beta-amyloid by solution-state NMR upon variation of salt conditions. *Biochemistry* 44: 1444–1452.
29. Pelton JG, Torchia DA, Meadow ND, Roseman S (1993) Tautomeric states of the active-site histidines of phosphorylated and unphosphorylated IIIIGlc, a signal-transducing protein from *Escherichia coli*, using two-dimensional hetero-nuclear NMR techniques. *Protein Sci* 2: 543–558.
30. Urbani A, Bazzo R, Nardi MC, Cicero DO, De Francesco R, et al. (1998) The metal binding site of the hepatitis C virus NS3 protease: A spectroscopic investigation. *J Biol Chem* 273: 18760–18769.
31. Blomberg F, Maurer W, Rueterjans H (1977) Nuclear magnetic resonance investigation of nitrogen-15-labeled histidine in aqueous solution. *J Am Chem Soc* 99: 8149–8159.
32. Hwang TL, van Zijl PCM, Mori S (1998) Accurate Quantitation of Water-amide Proton Exchange Rates Using the Phase-Modulated CLEAN Chemical EXchange (CLEANEX-PM) Approach with a Fast-HSQC (FHSQC) Detection Scheme. *J Biomol NMR* 11: 221–226.
33. Jarvet J, Danielsson J, Damberg P, Oleszczuk M, Gräslund A (2007) Positioning of the Alzheimer Abeta(1–40) peptide in SDS micelles using NMR and paramagnetic probes. *J Biomol NMR* 39: 63–72.
34. Hoyer W, Grönwall C, Jonsson A, Ståhl S, Hård T (2008) Stabilization of a beta-hairpin in monomeric Alzheimer's amyloid-beta peptide inhibits amyloid formation. *Proc Natl Acad Sci U S A* 105: 5099–5104.
35. Lazo ND, Grant MA, Condrón MC, Rigby AC, Teplow DB (2005) On the nucleation of amyloid beta-protein monomer folding. *Protein Sci* 14: 1581–1596.
36. Petkova AT, Ishii Y, Balbach JJ, Antzutkin ON, Leapman RD, et al. (2002) A structural model for Alzheimer's beta -amyloid fibrils based on experimental constraints from solid state NMR. *Proc Natl Acad Sci U S A* 99: 16742–16747.
37. Lührs T, Ritter C, Adrian M, Riek-Loher D, Bohrmann B, et al. (2005) 3D structure of Alzheimer's amyloid-beta(1–42) fibrils. *Proc Natl Acad Sci U S A* 102: 17342–17347.
38. Andreetto E, Yan LM, Tatarek-Nossol M, Velkova A, Frank R, et al. (2010) Identification of hot regions of the Abeta-IAPP interaction interface as high-affinity binding sites in both cross- and self-association. *Angew Chem Int Ed Engl* 49: 3081–3085.
39. Williamson MP, Suzuki Y, Bourne NT, Asakura T (2006) Binding of amyloid beta-peptide to ganglioside micelles is dependent on histidine-13. *Biochem J* 397: 483–490.
40. Yu L, Edalji R, Harlan JE, Holzman TF, Lopez AP, et al. (2009) Structural characterization of a soluble amyloid beta-peptide oligomer. *Biochemistry* 48: 1870–1877.
41. Bieschke J, Russ J, Friedrich RP, Ehrnhoefer DE, Wobst H, et al. (2010) EGCG remodels mature alpha-synuclein and amyloid-beta fibrils and reduces cellular toxicity. *Proc Natl Acad Sci U S A* 107: 7710–7715.